JOURNAL OF AGRICULTURAL AND FOOD CHEMISTRY

pubs.acs.org/JAFC Article

Action Mode of the Mycotoxin Patulin as a Novel Natural Photosystem II Inhibitor

Yanjing Guo, Weizhe Liu, He Wang, Xiaoxiong Wang, Sheng Qiang, Hazem M. Kalaji, Reto Jörg Strasser, and Shiguo Chen*

Cite This: J. Agric. Food Chem. 2021, 69, 7313−7323

ABSTRACT: A biocontrol method plays an important role in weed management. In this study, we aimed to clarify the phytotoxicity of the mycotoxin patulin (PAT) and reveal its mode of action as a new natural photosystem II (PSII) inhibitor. Phytotoxicity test showed that PAT has herbicidal activity and causes significant leaf lesions on *Ageratina adenophora*. Under a half-inhibition concentration I_{50} (2.24 μM), the observed significant decrease in oxygen evolution rate and the increase in the J-step of the chlorophyll fluorescence rise OJIP curve indicated that PAT strongly reduces photosynthetic efficiency by blocking electron transport from the primary to secondary plastoquinone acceptors (Q_A to Q_B) of PSII. Molecular modeling of PAT docking to the *A. adenophora* D1 protein suggested that PAT bounds to the Q_B site by forming hydrogen bonds to histidine 252 in the D1 protein. It is proposed that PAT is a new natural PSII inhibitor and has the potential to be developed into a bioherbicide or used as a template scaffold for discovering novel derivatives with more potent herbicidal activity.

KEYWORDS: *nature product, bioherbicide, chlorophyll a fluorescence, JIP-test, D1 protein, molecular docking*

INTRODUCTION

Chemical herbicides are widely used in agriculture and other fields, but their harmfulness to human health is receiving increasing attention. In addition, herbicide-resistant weeds are widely cultivated, which reduce the quality and yield of crops.[1] Consequently, research on bioherbicides becomes urgent due to their extensive resources, low toxicity, novel structures, unique targets, and environmentally friendly properties.[2]

Currently, biocontrol plays an important role in weed control compared to classical chemical herbicide control. The exploration of natural compounds is one of the most important approaches of bioherbicide development.[2] As the U.S. Environmental Protection Agency reported, during the period 1997 to 2010, nearly 70% of active pesticide ingredients that are newly registered are from natural products; thereinto, conventional herbicides for weed management derived from natural compounds account for 8%.[3] New natural compounds extracted from plants and microorganisms are important resources for the discovery of novel herbicidal ingredients and action targets.[4,5]

Until now, there are at least 25 different molecular targets for all commercial organic herbicides based on the latest classification of the Herbicide Resistance Action Committee (HRAC) (www.hracglobal.com). For herbicide action, chloroplasts are the most vital organelles since they are the cellular locations of 15 herbicide primary targets. This suggests that chloroplasts play a central function as photosynthetic apparatuses in the plant mechanism. This situation also explains why photosynthesis is often selected as the first priority, while a study was performed to probe the action target of a new product. In fact, the percentage of commercial photosynthesis-inhibiting herbicides takes up over 50% in the market.[6] Among them, the classical photosystem II (PSII)-inhibiting herbicides are classified into two groups based on chemical characteristics and inhibitory patterns: urea/triazine family possessing a common N—C═X group (e.g., diuron and atrazine), where X refers to N or O or C, and phenol family containing an aromatic hydroxyl group (e.g., bromoxynil and ioxynil). They inhibit photosynthesis by interrupting PSII electron transfer from primary plastoquinone Q_A to secondary plastoquinone Q_B.[7,8] There are also a few reports about natural PSII-inhibiting products isolated from plant or microbe organisms. For example, tenuazonic acid (TeA), a mycotoxin with a N—C═O moiety generated by the fungus *Alternaria alternata*, blocks PSII electron transfer further than Q_A at the acceptor side.[9] Gliotoxin with a characteristic group N—C═O, being extracted from fungi such as *Trichoderma* and *Aspergillus fumigatus*, inhibits PSII electron flow beyond Q_A and decreases the PSII oxygen evolution rate.[10] Stigmatellin, as a myxobacterium *Stigmatella aurantiaca*-produced antibiotic, has two inhibition sites as reported. One is located at the PSII-reducing side, and another is located at the cytochrome b6f (Cyt_b6f) complex.[11] Sorgoleone, an oxidized state of a hydrophobic *p*-benzoquinone, was obtained from root exudates of *Sorghum bicolor* and blocks the re-oxidation of

Received: March 29, 2021
Revised: June 5, 2021
Accepted: June 11, 2021
Published: June 24, 2021

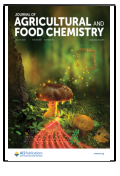

https://doi.org/10.1021/acs.jafc.1c01811
J. Agric. Food Chem. 2021, 69, 7313−7323

Q_A^- in PSII but has no effect on PSI.[12,13] Capsaicin, a natural quinone analog extracted from red pepper species, has the structure characteristics of both urea/triazine and phenol-type PSII inhibitors since it possesses vanilloid, amide, and hydrophobic side chains at the same time.[14] Fischerellin A, a cyanobacterium *Fischerella muscicola*-produced secondary metabolite, exhibits strong inhibition of PSII activity.[15]

Patulin (PAT, $C_7H_6O_4$), as a mycotoxin discovered mostly in apples and apple-derived products, is generated by molds *Penicillium*, *Aspergillus*, *Byssochlamys*, and so on.[16−18] It is reported that PAT caused cytotoxin-involving reactive oxygen species (ROS) generation, cytochrome c release in mitochondria, cytosolic Ca^{2+} uptake, activation of caspase-3, cell cycle arrest, and cell apoptosis.[19] Additionally, PAT can lead to DNA destruction, chromosome abnormality, and occurrence of micronuclei in mammalian cells.[20,21] Early in past century, PAT was reported to be potent in inhibiting seed germination as well as seedling growth of wheat, showing an interesting herbicide activity.[22] However, the physiological−biochemical mechanism and action target of PAT on plants remain unknown.

The chemical structure of PAT possesses an aromatic hydroxyl group that is a characteristic element of the phenol family of PSII herbicides. In this study, we aim to assess the phytotoxicity of PAT on various plant species and probe its mode of action in *A. adenophora* PSII. To evaluate the impact of PAT on photosynthetic activity, we measured chlorophyll (Chl) *a* fluorescence signals and the oxygen evolution rate and analyzed the fast Chl fluorescence rise kinetics to ensure the action sites of PAT on photosynthesis. By simulating the modeling of PAT binding to the D1 protein of *A. adenophora*, we further explored the accurate action target of PAT in the photosynthetic apparatus. Clarification of the action mode of PAT will allow the development of new valid herbicides or the design of efficient derivatives based on the PAT structure.

MATERIALS AND METHODS

Plants and Chemicals. Among 62 kinds of plants, *Microstegium vimineum*, *Digitaria sanguinalis*, *Eclipta prostrata*, *Zea mays*, *Triticum aestivum*, *Arachis hypogaea*, *Capsicum annuum*, *Gossypium barbadense*, and *Nicotiana tabacum* were cultivated in soil from seeds in the greenhouse for at least 30 days at 20−25 °C with white light of 200 μmol (photons) m^{-2} s^{-1} in the 12:12 h photoperiod. The invasive weed *A. adenophora* was grown for 180 days by rooting in perlite−vermiculite−peat mixtures (0.5:1:3, v/v) at 20−25 °C under white light (200 μmol m^{-2} s^{-1}) with a 12 h photoperiod and 70% relative humidity in the greenhouse. The rest of 62 species of plants were directly sampled from the local environments in Nanjing, China. The top second and third healthy leaves from all prepared plant species were collected for the following test.

PAT was obtained from Aladdin (CAS no. 149-29-1). It was dissolved with methanol as 20 mM and stocked in 4 °C. Diuron (3-(3,4-dichlorophenyl)-1,1-dimethylurea, DCMU), methyl viologen (MV), 2,6-dichloroindophenol (DCPIP), and other chemical reagents were purchased from Sigma-Aldrich (Shanghai, China).

Phytotoxicity Assessment *In Vitro*. Intact leaves detached from healthy plants of 62 species were washed with distilled water, dried with sterilized-filter papers, and transferred onto wet sterilized-filter papers in Petri dishes. Leaves were slightly punctured on their abaxial margin with a needle. A 20 μL droplet of 4000 μM PAT solution was added onto the wound site of leaves. All samples were maintained in a growth chamber at 25 °C for 48 h under white light (200 μmol m^{-2} s^{-1}) for a 12:12 h photoperiod. A vernier caliper (ROHS HORM 2002/95/EC, Xifeng, China) was used to determine the lesion diameter in leaves. The average size was calculated according to the longest and shortest diameters of leaf lesions. Each value is the average of at least 10 leaf samples. Phytotoxicity was assessed on the basis of a necrotic symbolic scale. Four levels of phytotoxicity, "−, +, + +, and +++", correspond respectively to four ranges of the leaf lesion area, "0 to <1, 1 to <10, 10 to <40, and ≥40 mm^2".

Phytotoxic Activity *In Vivo*. Plants *A. adenophora*, *Amaranthus retroflexus*, *M. vimineum*, *D. sanguinalis*, *Oryza sativa*, and *T. aestivum* were cultured at 25 °C under white light (200 μmol m^{-2} s^{-1}) in the 12:12 h photoperiod and 70% relative humidity in the greenhouse. Seedlings with two to three true leaves were sprayed to runoff with 1.8 mL of 0 (control, 0.1% methanol), 250, 500, 1000, and 2000 μM PAT solution (containing ≤0.1% methanol) utilizing a mist sprayer (SKS Bottle & Packaging Inc., NY, USA). Phytotoxicity was recorded with a Canon G15 camera (Canon, Tokyo, Japan) after 14 day treatment and quantified using the disease index according to Lô-Pelzer et al.[23]

Chl Fluorescence Imaging. Chl fluorescence imaging was measured by a MAXI-version of the pulse-modulated Imaging-PAM M-series fluorometer (Heinz Walz GmbH, Effeltrich, Germany).[24] For the measurement, the detached leaves of *A. adenophora* were punctured slightly on their abaxial margin with a needle. Twenty microliters of PAT solution with a 0 (control, 0.1% methanol), 500, 1000, 2000, 3000, or 4000 μM concentration was dripped onto the punctured wound. After 12 h treatment, fluorescence images were measured. Before the measurements, samples were adapted for 30 min in the dark under the imaging system camera after focusing the camera. The intensity of measuring light was set as 0.25 μmol (photons) m^{-2} s^{-1}; meanwhile, that of saturation pulse light was set as 6000 μmol (photons) m^{-2} s^{-1} during fluorescence imaging monitoring. Additionally, normal images were recorded with a digital camera and diameters of leaf necrotic lesions were also measured with calipers.

Determination of Photosynthetic Electron Transfer Activity. The photosynthetic electron transport chain was divided into five phases with various artificial electron donors and acceptors, and their activities were determined with a Clark-type oxygen electrode (Hansatech Instruments Ltd., King's Lynn, U.K.) according to Coombs et al.[25] Thylakoid membranes of *A. adenophora* leaves were extracted referring to Chen et al.[26] PAT was added into 0.25 mL of thylakoid suspension (containing 50 μg of chlorophylls) to give PAT concentrations of 1, 2, 10, 20, 40, 80, and 100 μM. The mixtures were kept for 30 min in the darkness at 4 °C and then added into various reaction media. The phase 1, referring to the activity of the whole electron transfer chain from H_2O to the PSI reaction center P_{700}, was measured in a reaction medium containing 60 mM Tris (pH = 7.5), 20 mM $NaHCO_3$, 5 mM NH_4Cl, 2 mM sodium azide, and 50 μM MV as electron acceptors. The phase 2, reflecting the activity of the PSI electron transfer chain, was determined using DCPIP as donors and MV as acceptors in a reaction system involving 60 mM Tris (pH = 7.5), 20 mM $NaHCO_3$, 5 mM NH_4Cl, 2 mM sodium azide, 2 mM L-ascorbic acid sodium salt, 50 μM MV, and 50 μM DCMU. The phase 3, representing the activity of PSII involving a DCMU-sensitive site, was determined using H_2O as donors and phenylenediamine as acceptors in a reaction system containing 60 mM Tris (pH = 7.5), 20 mM $NaHCO_3$, 5 mM NH_4Cl, 4 mM potassium ferricyanide, and 1 mM phenylenediamine. The phase 4, meaning the activity of PSII without a DCMU-sensitive site, was measured using H_2O as donors and silicomolybdate as acceptors in a reaction medium containing 60 mM HEPES-KOH (pH = 7.0), 20 mM $NaHCO_3$, 0.5 mM potassium ferricyanide, 5 μM DCMU, and 0.1 mM silicomolybdate. The phase 5, reflecting the total activity of PSII and PSI but without a water splitting complex, was measured in the existence of sym-diphenylcarbazide (DPC) as donors and MV as acceptors in a reaction system containing 60 mM Tris (pH = 7.5), 20 mM $NaHCO_3$, 5 mM NH_4Cl, 2 mM sodium azide, 50 μM MV, and 0.5 mM DPC. Samples were then exposed to red light illumination (400 μmol m^{-2} s^{-1}). The activity of electron transport was determined during the first 3 min after the onset of illumination.

Determination of Fast Chl Fluorescence Rise Kinetics and JIP-Test Analysis. Chl fluorescence rise OJIP curves were measured by a plant efficiency analyzer (Hansatech Instruments Ltd., King's Lynn, U.K.). Seven millimeter-diameter leaf discs from *A. adenophora*

https://doi.org/10.1021/acs.jafc.1c01811
J. Agric. Food Chem. 2021, 69, 7313−7323

plants were prepared and immersed in PAT solutions with 0 (0.1% methanol), 25, 50, 100, or 200 μM concentrations or in 100 μM DCMU solution for 12 h, respectively. Leaf discs were also incubated in 200 μM PAT solutions for 0, 3, 6, and 12 h. Samples were well dark-adapted before the measurements and exposed to continuous red light illumination (650 nm, 3500 μmol m^{-2} s^{-1}). Experiments were replicated three times with at least 15 repetitions. Based on the model of "Theory of Energy Fluxes in Biomembranes", the fluorescence rise OJIP curves were analyzed using the JIP-test.[27] This analysis took into consideration several basic fluorescence data at 20 μs (F_O), at 300 μs (F_K), at 2 ms (F_J), at 30 ms (F_I), and at the maximum (F_M, which is equal to F_P). V_t, calculated by the formula $V_t = (F_t - F_O)/(F_M - F_O)$, represents relative variable fluorescence at time t. Detailed parameters are listed in Table 1, where formulas, equations, and definitions of JIP-test parameters are listed according to Strasser et al. and Chen et al.[27,28]

Modeling of PAT in the Q_B Site. The amino acid sequence of the target protein D1 of *A. adenophora* (reference sequence no. YP 004564352.1) was obtained from NCBI, which served as a query in searching for evolutionary-related proteins with available structures by the BLAST program through the SWISS-MODEL Template Library.[29] The searching templates of the D1 protein were estimated using Global Model Quality Estimate and Quaternary Structure Quality Estimate and ranked according to the model quality. The protein structures of the top ranked templates were downloaded from the Protein Data Bank and then used to produce the homology model of the *A. adenophora* D1 protein by the Protein Modeling Module of Discovery Studio. ChemBioDraw Ultra 14.0 software (CambridgeSoft, America) was used to construct the chemical structure of PAT, which was energetically minimized by MM2 energy minimizations in Chem3D Pro 14.0 (CambridgeSoft, America). DS-CDocker in Discovery Studio 3.5 (BIOVIA, America) was utilized to perform the docking. During energy minimization and molecular refinement, the polar hydrogens were added to the protein.

RESULTS AND DISCUSSION

Phytotoxicity of PAT to Various Plant Species. Sixty-two kinds of plants were evaluated and classified into four classes according to their different responses to 4000 μM PAT that is reflected by the size of the leaf lesion (Table 2). Highly susceptible species included *M. vimineum*, *A. adenophora*, *Carpesium abrotanoides*, *Youngia japonica*, *E. prostrata*, *Solidago canadensis*, *Glycine max*, *Solanum lyratum*, *Broussonetia papyrifera*, *Plantago asiatica*, *Cayratia japonica*, and *Thyrocarpus sampsonii*, a total of 12 species. After PAT treatment, over 40 mm^2 necrotic lesions on their leaves were formed. Among them, *A. adenophora* with a 211 mm^2 leaf lesion exhibited the highest susceptibility, which is a notorious invasive weed worldwide that originated from Mexico and actually leads to serious local ecosystem destruction along with economic loss in the southwest of China.[30] There are 31 moderate susceptible species with 10−40 mm^2 necrotic lesions, including the common agricultural weeds, such as *Poa pratensis*, *Setaria viridis*, *D. sanguinalis*, *Erigeron annuus*, *Conyza canadensis*, *Alternanthera philoxeroides*, *Polygonaceae*, *Veronica hederaefola*, *Humulus scandens*, and *Monochoria vaginalis*. In addition, eight species including four crops (*O. sativa*, *T. aestivum*, *Morus alba*, and *G. barbadense*) belong to the low susceptible plants with leaf necrotic lesions of 1 to 10 mm^2 after PAT treatment. It was also observed that *Z. mays*, *Ginkgo biloba*, and the other nine plant species are highly tolerant to PAT. Only less than 1 mm^2 necrotic lesions on their leaves were formed in the presence of PAT. It is clear that 43 of 62 plant species showed excellent susceptibility to PAT, especially weeds of Compositae and Gramineae families. PAT exhibits a broad spectrum for weed control.

Table 1. Formulae and Explanation of the Technical Data of the Fluorescence Rise OJIP Curve and the Selected JIP-Test Parameters Used in This Research[a]

technical fluorescence parameters	
F_t	fluorescence at time t after the onset of actinic illumination
$F_O \cong F_{20\mu s}$	minimal fluorescence when all PSII RCs are open
$F_L \equiv F_{150\mu s}$	fluorescence intensity at the L-step (150 μs) of OJIP
$F_K \equiv F_{300\mu s}$	fluorescence intensity at the K-step (300 μs) of OJIP
$F_J \equiv F_{2ms}$	fluorescence intensity at the J-step (2 ms) of OJIP
$F_I \equiv F_{30ms}$	fluorescence intensity at the I-step (30 ms) of OJIP
F_P (= F_M)	maximal fluorescence, at the peak P of OJIP
$F_v \equiv F_t - F_O$	variable fluorescence at time t
$V_t \equiv (F_t - F_O)/(F_M - F_O)$	relative variable fluorescence at time t
$V_J = (F_J - F_O)/(F_M - F_O)$	relative variable fluorescence at the J-step
$W_t \equiv (F_t - F_O)/(F_J - F_O)$	relative variable fluorescence F_v to the amplitude $F_J - F_O$
$W_{OJ} = (F_t - F_O)/(F_J - F_O)$	ratio of variable fluorescence $F_t - F_O$ to the amplitude $F_J - F_O$
quantum efficiencies or flux ratios	
$\varphi_{Po} = PHI(P_0) = TR_0/ABS = 1 - F_O/F_M$	maximum quantum yield for primary photochemistry
$\psi_{Eo} = PSI_0 = ET_0/TR_0 = (1 - V_J)$	probability that an electron moves further than Q_A^-
$\varphi_{Eo} = PHI(E_0) = ET_0/ABS = (1 - F_O/F_M)(1 - V_J)$	quantum yield for electron transport (ET)
$\gamma_{RC} = Chl_{RC}/Chl_{total} = RC/(ABS + RC)$	probability that a PSII Chl molecule functions as RC
phenomenological energy fluxes (per excited leaf cross section (CS))	
$ABS/CS = Chl/CS$	absorption flux per CS
$TR_0/CS = \varphi_{Po}\cdot(ABS/CS)$	trapped energy flux per CS
$ET_0/CS = \varphi_{Po}\cdot\psi_{Eo}\cdot(ABS/CS)$	electron transport flux per CS
density of reaction center (Q_A-reducing PSII reaction center (RC))	
$RC/CS = \varphi_{Po}\cdot(V_J/M_0)\cdot(ABS/CS)$	density of Q_A-reducing PSII RCs per CS
Q_A-reducing centers = $\frac{RC}{RC_{reference}}\cdot\frac{ABS}{ABS_{reference}} = \frac{(RC/CS)_{treatment}}{(RC/CS)_{control}}\cdot\frac{(ABS/CS)_{treatment}}{(ABS/CS)_{control}}$	fraction of Q_A-reducing PSII RCs
$R_J = \frac{\psi_{Eo(control)} - \psi_{Eo(treatment)}}{\psi_{Eo(control)}} = \frac{V_{J(treatment)} - V_{J(control)}}{1 - V_{J(control)}}$	number of PSII RCs with the Q_B site filled by the PSII inhibitor
OEC centers = $\frac{1 - (V_K/V_J)_{treatment}}{1 - (V_K/V_J)_{control}}$	the active fraction of oxygen evolving complex centers
performance indexes	
$PI_{ABS} \equiv \frac{\gamma_{RC}}{1-\gamma_{RC}}\cdot\frac{\varphi_{Po}}{1-\varphi_{Po}}\cdot\frac{\psi_{Eo}}{1-\psi_{Eo}}$	performance index for energy conservation from photons absorbed by PSII to the reduction of intersystem electron acceptors

[a]Subscript "0" or "o" means that the parameter refers to the onset of illumination when all RCs are assumed to be open.

To further assess effects of PAT on weeds and crops, the seedlings of *A. adenophora*, *A. retroflexus*, *M. vimineum*, *D. sanguinalis*, *O. sativa*, and *T. aestivum* at the two- to three-leaf stage were treated with 0, 250, 500, 1000, and 2000 μM PAT solutions, respectively, and treated for 14 days (Figure 1A). For *A. adenophora* and *M. vimineum*, PAT with a low concentration of 500 μM almost caused the total death of the seedlings and the disease indexes reached to 100 and 92, respectively. The disease indexes of PAT on *A. retroflexus* and

https://doi.org/10.1021/acs.jafc.1c01811
J. Agric. Food Chem. 2021, 69, 7313−7323

Table 2. Phytotoxicity of Patulin (PAT) to Different Plants *In Vitro*[b]

family	plant species	lesion area (mm^2)	path. level[a]	family	plant species	lesion area (mm^2)	path. level[a]
Gramineae	*Microstegium vimineum*	41.31 ± 0.12	+++	Polygonaceae	*Polygonaceae*	35.64 ± 0.18	++
	Poa pratensis	17.90 ± 0.06	++		*Fallopia multiflora*	14.86 ± 0.12	++
	Lolium perenne	15.43 ± 0.09	++		*Polygonum longisetum*	0.14 ± 0.08	−
	Setaria viridis	13.52 ± 0.03	++	Lamiaceae	*Perilla frutescens*	30.25 ± 0.16	++
	Digitaria sanguinalis	12.58 ± 0.13	++		*Lamium barbatum*	21.50 ± 0.15	++
	Oryza sativa	8.46 ± 0.13	+		*Glechoma longituba*	17.90 ± 0.21	++
	Triticum aestivum	4.60 ± 0.18	+	Amaranthaceae	*Alternanthera philoxeroides*	18.87 ± 0.11	++
	Zea mays	0.66 ± 0.02	−		*Achyranthes bidentata*	14.86 ± 0.12	++
Compositae	*Ageratina adenophora*	211.08 ± 0.19	+++	Scrophulariaceae	*Veronica hederaefola*	18.00 ± 0.15	++
	Carpesium abrotanoides	45.60 ± 0.12	+++	Moraceae	*Broussonetia papyrifera*	42.24 ± 0.19	+++
	Youngia japonica	44.60 ± 0.18	+++		*Humulus scandens*	26.17 ± 0.12	++
	Eclipta prostrata	41.35 ± 0.04	+++		*Morus alba*	4.49 ± 0.14	+
	Solidago Canadensis	40.44 ± 0.18	+++	Rosaceae	*Duchesnea indica*	10.50 ± 0.08	++
	Kalimeris indica	29.10 ± 0.13	++		*Rubus parvifolius*	0.18 ± 0.12	−
	Pterocypsela indica	25.19 ± 0.25	++	Malvaceae	*Gossypium barbadense*	9.86 ± 0.12	+
	Bidens pilosa	21.12 ± 0.14	++	Plantaginaceae	*Plantago asiatica*	41.50 ± 0.02	+++
	Erigeron annuus	10.88 ± 0.10	++	Geraniaceae	*Geranium wilfordii*	9.11 ± 0.15	+
	Conyza canadensis	10.46 ± 0.07	++	Vitaceae	*Cayratia japonica*	41.27 ± 0.16	+++
	Xanthium sibiricum	0.24 ± 0.12	−	Boraginaceae	*Thyrocarpus sampsonii*	66.10 ± 0.12	+++
Leguminosae	*Glycine max*	46.44 ± 0.18	+++	Oxalidaceae	*Oxalis corniculata*	20.80 ± 0.15	++
	Arachis hypogaea	19.90 ± 0.19	++	Nyctaginaceae	*Mirabilis jalapa*	0.54 ± 0.08	−
	Medicago sativa	19.20 ± 0.05	++	Meliaceae	*Melia azedarach*	18.46 ± 0.07	++
	Wisteria sinensis	15.90 ± 0.14	++	Oleaceae	*Jasminum nudiflorum*	0.44 ± 0.12	−
	Trifolium repense	4.30 ± 0.17	+	Umbelliferae	*Hydrocotyle sibthorpioides*	0.62 ± 0.16	−
Convolvulaceae	*Pharbitis nil*	34.24 ± 0.16	++	Sterculiaceae	*Melochia corchorifolia*	7.99 ± 0.05	+
	Dichondra repens	16.10 ± 0.06	++	Celastraceae	*Euonymus fortunei*	0.24 ± 0.12	−
Solanaceae	*Solanum lyratum*	64.73 ± 0.14	+++	Pontederiaceae	*Monochoria vaginalis*	20.16 ± 0.02	++
	Capsicum annuum	26.19 ± 0.25	++	Liliaceae	*Ophiopogon bodinieri*	0.35 ± 0.08	−
	Nicotiana tabacum	14.86 ± 0.17	++	Ginkgoaceae	*Ginkgo biloba*	0.06 ± 0.08	−
Euphorbiaceae	*Acalypha australis*	17.39 ± 0.04	++	Pteridaceae	*Pteris ensiformis*	9.08 ± 0.03	+
	Sapium sebiferum	13.05 ± 0.06	++	Lygodiaceae	*Lygodium japonicum*	0.08 ± 0.06	−

[a]Pathogenicity levels "−, +, ++, and +++" denote leaf lesion areas of 0 to <1 mm^2, 1 to <10 mm^2, 10 to <40 mm^2, and ≥40 mm^2, respectively. [b]Intact leaves detached from healthy plants of different species are rinsed with distilled water, dried with sterilized-filter papers, and subsequently placed onto wet sterilized-filter papers in Petri dishes. The leaves were slightly punctured on their abaxial margin with a needle. A 20 μL droplet of 4000 μM PAT solution was added onto the wound site of leaves. All samples were incubated in a growth chamber at 25 °C for 48 h under white light (200 μmol m^{-2} s^{-1}) with a 12:12 h photoperiod. The area of the leaf lesion was determined with calipers. Each value is the average of at least 10 leaf samples.

D. sanguinalis exhibited a concentration-dependent increase, which reached beyond 98 and 100 in the case of 2000 μM PAT treatment. However, for crops *O. sativa* and *T. aestivum*, the disease indexes are just 1.93 and 2.28 after treatment of the highest concentration of 2000 μM PAT (Figure 1B).

Above results suggest that PAT has the potential to be developed into a bioherbicide for the control of the invasive alien weed *A. adenophora* or grass and broadleaf weeds in maize.

PAT Caused Leaf Lesions of *A. adenophora* Due to Photosynthetic Damage. To further estimate the phytotoxicity of PAT, a lesion formation in the detached mature leaves of *A. adenophora* was monitored after PAT treatment with various concentrations for 6 to 24 h. As a result, a visible concentration-dependent development of the leaf necrotic lesion was observed at 12 h (Figure 2A). By increasing the PAT treatment concentration and time, the size of the leaf lesion increased quickly (Figure 2B). In fact, necrotic and chlorotic lesions were the common symptoms in PAT-treated leaves or seedlings. It is noticeable that PAT caused necrosis in *A. adenophora* and *M. vimineum* seedlings and bleaching in *A. retroflexus* and *D. sanguinalis* seedlings (Figure 1A). The occurrence of necrotic or chlorotic lesions means a serious damage on photosynthetic tissues due to chlorophyll breakup.[10] To verify the influence of PAT on the photosynthetic apparatus, the damage caused by PAT on *A. adenophora* leaves was monitored by the Imaging-PAM Chl fluorometer. The color-coded images of F_V/F_M, the maximal quantum yield of PSII, gradually changed from blue in the control to black at the highest concentration of PAT after 12 h treatment (Figure 2C). Obviously, PAT dramatically decreased the photosynthetic activity.

PAT Inhibited PSII Electron Transport. The plant photosynthetic apparatus consists of two systems of PSII and PSI that are located in the thylakoid membranes. Light energy is absorbed by chlorophylls and transferred to the PSII reaction center P_{680} and PSI reaction center P_{700}, which dives electron flow from H_2O to $NADP^+$ via tyrosine, P_{680}, and different intermediate carriers including Pheo (primary electron acceptor pheophytin), Q_A and Q_B, plastoquinone PQ_t FeS (iron−sulfur protein), Cyt_b6f (cytochrome b6f), PC (plastocyanin), P_{700}, Fd (ferredoxin), and FNR (ferredoxin-$NADP^+$ reductase). This is the well-known Z-scheme photosynthetic electron transport.[31]

https://doi.org/10.1021/acs.jafc.1c01811
J. Agric. Food Chem. 2021, 69, 7313−7323

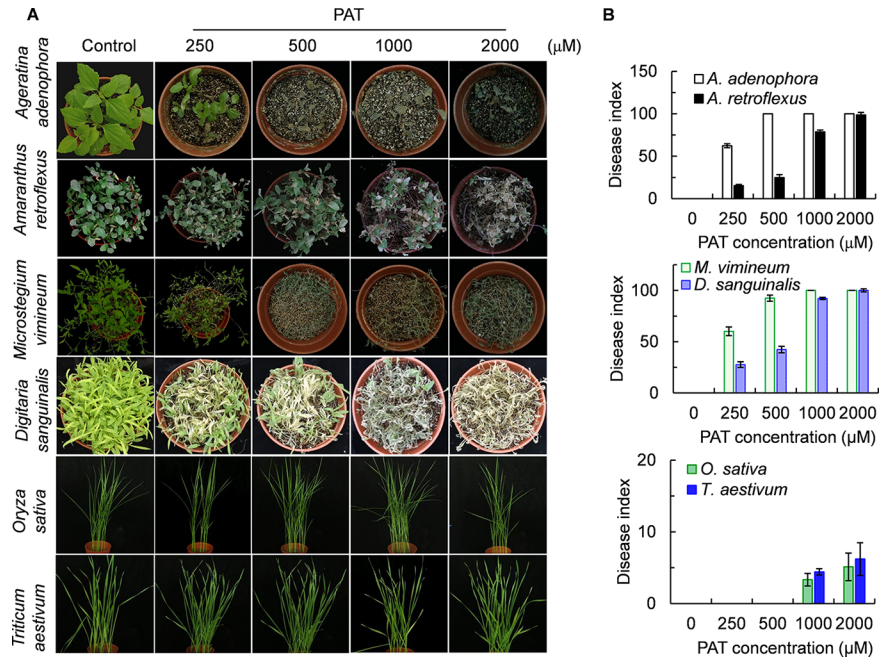

Figure 1. Whole plant phytotoxicity of patulin (PAT) on *A. adenophora*, *A. retroflexus*, *M. vimineum*, *D. sanguinalis*, *O. sativa*, and *T. aestivum*. Seedlings were sprayed to runoff with a solution containing 0, 250, 500, 1000, and 2000 μM PAT and maintained for 14 days at 25 °C under white light (200 μmol m^{-2} s^{-1}) in a chamber. (A) Photographs of six plants after PAT treatment. (B) Disease indexes of six plants after PAT treatment.

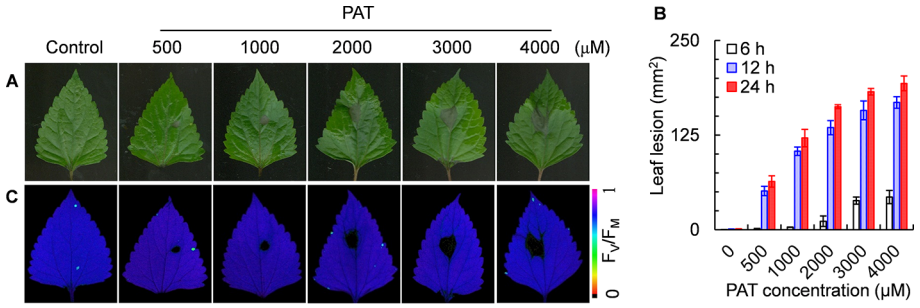

Figure 2. Patulin (PAT)-induced damage to *A. adenophora* leaf tissues. (A) Necrotic lesion formation of *A. adenophora* leaves incubated for 12 h with different concentrations of PAT (0, 500, 1000, 2000, 3000, and 4000 μM). (B) Size of the leaf lesion after 6 to 24 h PAT treatment with different concentrations. (C) Color fluorescence images of F_V/F_M in which the color code is in the order of black (0) via red, orange, yellow, green, blue, and violet to purple (1). Results shown are mean values ± SD of three independent biological replicates.

To probe the action site of PAT in two photosystems, the photosynthetic electron transport chain was divided into five phases to measure their activity by utilizing different artificial electron donors and acceptors according to Coombs et al.[25] (Figure 3A). After thylakoids of *A. adenophora* were incubated with different concentrations of PAT for 30 min, the activities of the whole electron transfer chain from H_2O to P_{700} (phase 1) and the PSII electron transfer chain from H_2O to phenylenediamine (phase 3), as well as the total activity of PSII and PSI except for the water splitting complex, which is from DPC and MV (phase 5), were measured, which showed a clear concentration-dependent decrease (Figure 3B,D,F). However, no distinct change in the activities of the PSI electron transfer chain and PSII electron transfer chain without a DCMU-sensitive site was observed (Figure 3C,E). Obviously, PAT inhibited PSII electron transport so that it led to a decrease in whole electron transfer activity. Moreover, PAT did not affect the electron transfer activity of the PSI and PSII donor side. It was indicated that the action site of PAT is just at the PSII acceptor side, which is similar to that of herbicide DCMU. Under DCMU treatment, electrons can hardly go pass Q_A to PSI because DCMU as an excellent photosynthetic inhibitor binding to the D1 protein entirely interrupts electron flow beyond Q_A.[27] As shown in Figure 3G, DCMU decreased the oxygen evolution rate of PSII and its I_{50} value was 0.12 μM. For PAT, the I_{50} value for the PSII oxygen evolution rate was calculated to be around 2.24 μM on the basis of the data from Figure 3D. This means that PAT is a little weaker PSII inhibitor relative to DCMU.

Compared with DCMU, most natural photosynthetic inhibiting products usually show lower inhibitory capability of PSII activity. Phytotoxin TeA and gliotoxin decrease the PSII oxygen evolution rate, respectively, with I_{50} values of 261 and 60 μM.[9,10] The I_{50} value of the quinone analog capsaicin for PSII electron transport at the acceptor side was determined to be about 12.6 μM.[14] Fischerellin A inhibits strongly the PSII oxygen evolution rate and has an I_{50} value of about 1 μM.[15] Obviously, PAT indeed exhibits a remarkable inhibitory activity on the PSII oxygen evolution rate at low concentrations. However, there are two more strong natural PSII

https://doi.org/10.1021/acs.jafc.1c01811
J. Agric. Food Chem. 2021, 69, 7313−7323

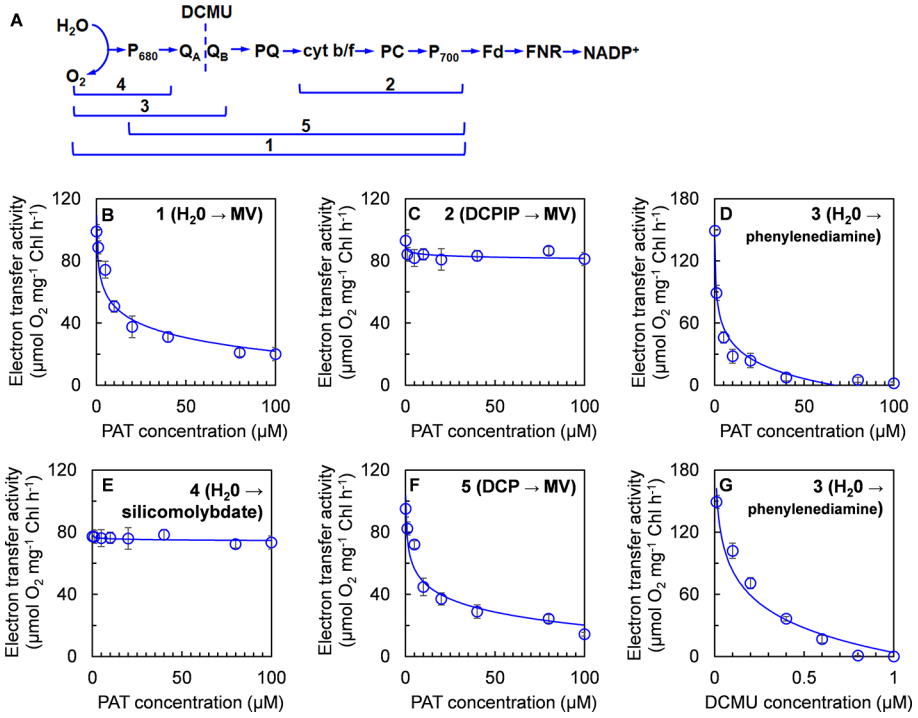

Figure 3. Impact of patulin (PAT) on the photosynthetic electron transport activity of *A. adenophora*. Thylakoids of *A. adenophora* were treated for 30 min with 0, 1, 2, 10, 20, 40, 80, and 100 μM PAT. (A) Schematic diagram of the photosynthetic electron transport chain that was divided into five phases to measure their activity by utilizing different artificial electron donors and acceptors. (B) Effect of PAT on the activity of the whole electron transfer chain from H_2O to P_{700}. (C) Effect of PAT on the activity of the PSI electron transfer chain from DCPIP to MV. (D) Effect of PAT on the activity of the PSII electron transfer chain from H_2O to phenylenediamine. (E) Effect of PAT on the activity of PSII without a DCMU-sensitive site from H_2O to silicomolybdate. (F) Effect of PAT on the activity of the total activity of PSII and PSI except for the water splitting complex, which is from DPC and MV. (G) Effect of different concentrations (0, 0.125, 0.25, 0.5, and 1 μM) of DCMU on the activity of the PSII electron transfer chain from H_2O to phenylenediamine. Each experiment was performed after at least three independent replicates.

inhibitors compared to PAT. One is sorgoleone, which blocks the re-oxidation of Q_A^- in PSII. Its I_{50} value was reported to be 0.1 μM that is equal to that of DCMU.[13] Another is stigmatellin with two different inhibition sites. It has an I_{50} value of 52.5 nM for the reducing side of PSII and 59.0 nM for the Cyt_b6f complex.[11] So far, stigmatellin is considered as the strongest inhibitor of spinach photosynthetic electron transport.

Analysis of Fluorescence Rise Kinetic OJIP. As a non-invasive spectroscopic technique, fast Chl fluorescence rise kinetic OJIP has been extensively applied in the investigation *in vivo* of the structure, conformation, and function of photosynthetic apparatus and especially of PSII.[27,32] To further precisely probe the sites of action of PAT on PSII, the fluorescence rise OJIP curves of PAT- and DCMU-treated *A. adenophora* leaves were measured (Figure 4A,B). As shown in Figure 4A,B, the fluorescence rise curve of the control is a typical polyphasic O-J-I-P shape. DCMU and PAT treatment resulted in an evident change of the OJIP curve. Under 100 μM DCMU treatment, the J-step rose rapidly to the same level of F_M. The fast increase in J-step level is attributed to the large accumulation of Q_A^- in PSII reaction centers due to the blockage of the electron transfer beyond Q_A.[27,33] For PAT, it is clear that the maximal fluorescence value (F_M) and variable fluorescence intensity (F_t) decreased greatly, and the I- and P-steps disappeared gradually with treatment concentration and time increasing. Such a phenomenon is similar to gliotoxin. A remarkable increase in the J-step level and a visible decrease in F_M indicate that gliotoxin not only blocks PSII electron flow beyond Q_A but also damages the structure and function of PSII antennae.[10] In addition, the fluorescence rise OJIP curve of diterpene β-lactone-treated samples showed a clear decrease in F_M because it inhibited PSII electron transport from P_{680} to Q_A.[34]

To investigate the detailed internal impact of PAT on the fluorescence rise kinetic properties, each OJIP curve was double-normalized by F_O and F_M and was given as relative variable fluorescence $V_t = (F_t - F_O)/(F_M - F_O)$ (top) and $\Delta V_t = V_{t(treated)} - V_{t(control)}$ (bottom) versus logarithmic timescale (Figure 4C, "control" refers to the samples treated with 0.1% methanol). Clearly, a marked increase in the J-peak is the main effect of PAT on the fluorescence rise kinetics. This is indeed equivalent to the behavior of DCMU.[27] Additionally, PAT slightly decreased the K-step (Figure 4C). To further evaluate the effect of PAT on the K-step, normalization of O- and J-steps, $W_{OJ} = (F_t - F_O)/(F_J - F_O)$ (top) and $\Delta W_{OJ} = W_{OJ(treated)} - W_{OJ(control)}$ (bottom) in the linear timescale (10 μs to 2 ms), is presented to show the K-band (Figure 4D). It is known that the occurrence of the K-step is associated with the status of OEC activity. An increase in the amplitude of the K-step or ΔK peak reflects the degree of OEC injury.[27,35,36] Here, PAT showed a negative influence on the amplitude of the K-step (Figure 4D), leading to a slight increase in the active fraction of OEC centers (Figure 5D). This suggests that PAT may stimulate slightly the activity of OEC.

JIP-test is a powerful tool for analyzing fluorescence rise kinetic OJIP to quantify PSII behavior under different stresses.[27] It is clear that increasing the concentration of PAT had nearly no effect on F_O but decreased markedly the value of F_M (Figure 5A). The F_O of dark-adapted leaf samples

https://doi.org/10.1021/acs.jafc.1c01811
J. Agric. Food Chem. 2021, 69, 7313−7323

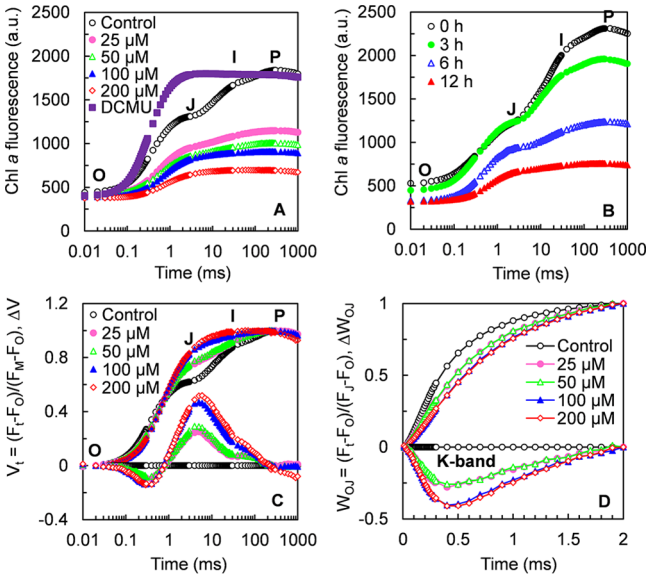

Figure 4. Effect of patulin (PAT) on the fluorescence rise kinetics of *A. adenophora*. (A) Fluorescence rise OJIP curves of leaves after 12 h treatment with 0.1% methanol (control), 100 μM DCMU, and PAT with different concentrations (25, 50, 100, and 200 μM). (B) Fluorescence rise OJIP curves of 200 μM PAT-treated leaves for different times (0, 3, 6, and 12 h). (C) Fluorescence rise kinetics double-normalized by F_O and F_M as $V_t = (F_t - F_O)/(F_M - F_O)$ (top) and $\Delta V_t = V_{t(\text{treatment})} - V_{t(\text{control})}$ (bottom) versus logarithmic timescale. (D) Fluorescence rise kinetics double-normalized by F_O and F_J as $W_{OJ} = (F_t - F_O)/(F_J - F_O)$ (top) and the difference kinetics $\Delta W_{OJ} = W_{OJ(\text{treatment})} - W_{OJ(\text{control})}$ (bottom) in the linear timescale to show K-band. Each curve is the average of 30 measurements.

reflects the PSII pigment property.[37] A decrease in F_M might be due to the oxidization of plastoquinone pool or destruction of the structure and function of PSII antennae.[38] An increase in the V_J value shows that PAT blocked PSII electron transport beyond Q_A (Figure 5B). This is further supported by the significant decrease in parameters φ_{Eo} and ψ_{Eo} (Figure 5C). φ_{Eo} refers to the quantum yield of PSII electron transport, whereas ψ_{Eo} reflects the probability that a trapped exciton moves an electron into the electron transport chain beyond Q_A.[27] A visible decrease in φ_{Po} was also observed after PAT treatment (Figure 5C), indicating the inhibition of the maximum quantum yield for PSII primary photochemistry. Since PAT interrupted PSII electron flow from Q_A to Q_B, inactivation events of PSII reaction centers are expected to occur. The fraction of Q_A-reducing centers could be obtained referring to Chen et al.,[28] with the following expression: Q_A-reducing centers $= \frac{(\text{RC}/\text{CS})_{\text{treatment}}}{(\text{RC}/\text{CS})_{\text{control}}} \cdot \frac{(\text{ABS}/\text{CS})_{\text{treatment}}}{(\text{ABS}/\text{CS})_{\text{control}}}$. The Q_A-reducing centers of PAT-treated leaves decreased around 59% (25 μM), 66% (50 μM), 72% (100 μM), and 83% (200 μM) compared with that of control (Figure 5D). This suggests that PAT really caused the quick closure of PSII reaction centers. It was demonstrated that fischerellin A increased the J-step significantly and inactivated the photosynthetic reaction centers in cyanobacteria, green algae, and pea leaves.[15] A distinct decrease in Q_A-reducing centers certainly makes an increase of non-Q_A-reducing centers that are also called heat sink centers, resulting in ROS generation.[27,28]

It has been proved that PSII inhibitors cause the inactivation of PSII reaction centers for interrupting electron transport further than Q_A due to their occupying positions of the Q_B-binding site in the D1 protein.[39,40] The fluorescence parameter R_J representing the number of PSII reaction centers with the Q_B site filled by PSII inhibitor molecules could be derived from the equation $R_J = \frac{V_{J(\text{treatment})} - V_{J(\text{control})}}{1 - V_{J(\text{control})}}$.[27,39] When leaf discs were

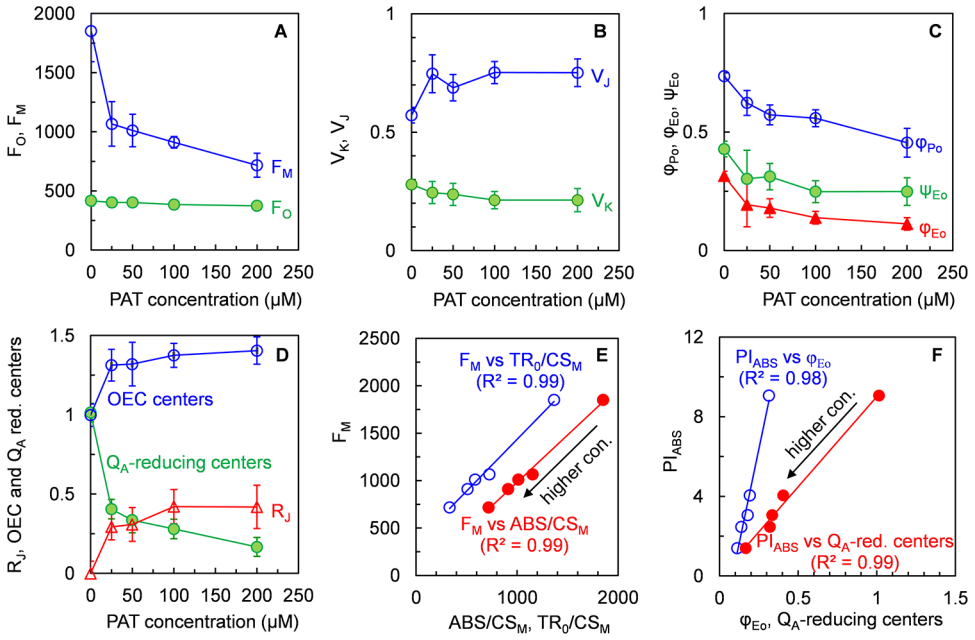

Figure 5. Effects of patulin (PAT) on the selected JIP-test parameters of *A. adenophora*. (A) Concentration-dependent effect on F_O and F_M. (B) Concentration-dependent effect on V_K and V_J. (C) Concentration-dependent effect on φ_{Po}, φ_{Eo}, and ψ_{Eo}. (D) Concentration-dependent effect on R_J, OEC centers, and Q_A-reducing centers. (E) Analysis of the correlation for F_M versus ABS/CS$_M$ and TR$_0$/CS$_M$. (F) Analysis of the correlation for PI$_{ABS}$ versus φ_{Eo} and Q_A-reducing centers. *A. adenophora* leaves were treated with 0, 25, 50, 100, and 200 μM PAT for 12 h. Each data is the average of 30 measurements.

https://doi.org/10.1021/acs.jafc.1c01811
J. Agric. Food Chem. 2021, 69, 7313−7323

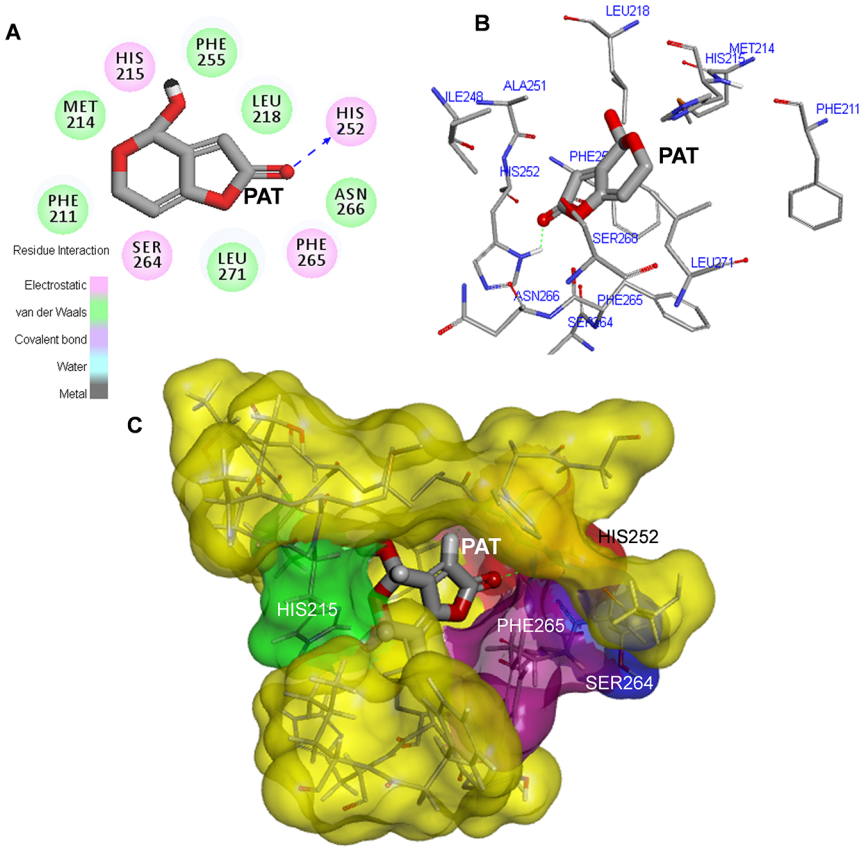

Figure 6. Simulated modeling of patulin (PAT) binding to the D1 protein of *A. adenophora*. (A) Hydrogen bonding interactions of PAT binding to the D1 protein. (B) Stereo view of the PAT binding environment of the D1 protein, in which carbon atoms are shown in gray, oxygen in red, nitrogen atoms in blue, and hydrogen atoms in white. The possible hydrogen bonds are marked by dashed lines. (C) Surface representation of the Q_B binding site with bound PAT.

Table 3. Possible Bonding Interactions for Patulin (PAT) Binding to the D1 Protein of *A. adenophora*

Com.	Mol. Formula	Chemical Structure	Donor	Acceptor	Interactions	Bound distance (Å)
Patulin (PAT)	$C_7H_6O_4$	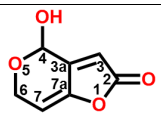	D1-His215	PAT O4	Electrostatic	3.11
			PAT O2	**D1-His 252 NH**	Hydrogen bond	2.24
			D1-Ser264	PAT C7	Electrostatic	2.83
			D1-Phe265	PAT O1	Electrostatic	3.14

incubated for 12 h with PAT, the number of PSII reaction centers with the Q_B site filled by PAT showed an approximately concentration-dependent enhancement (Figure 5D). So, it is concluded that PAT-caused inactivation of PSII reaction centers is possibly a result of PAT binding to the D1 protein.

Data in Figure 5E show that there is a linear relationship between F_M and ABS/CS_M or TR_0/CS_M in leaves treated with different concentrations of PAT. This indicates that the reduction of F_M is mainly caused by decreasing values of ABS/CS_M or TR_0/CS_M. ABS/CS_M expressing the total absorption flux per PSII cross section is regarded as an indicator for chlorophyll concentration or an average antenna size.[15,27] TR_0/CS_M reflecting the trapped energy flux per PSII cross section denotes the specific rate of the exciton trapped by open reaction centers.[27] A highly concentration-dependent decrease in ABS/CS_M and TR_0/CS_M suggested that PAT not only decreased the concentration of chlorophylls but also destroyed the conformation of the antenna pigment assemblies and reduced light energy transfer efficiency between antenna pigment molecules and from those to the PSII reaction centers. This is possibly due to the oxidative damage on the PSII structure for ROS production.

The performance index PI_{ABS}, as the most sensitive JIP-test parameter to various stresses, expresses the overall photosynthetic activity of PSII.[27] After leaves were exposed to PAT, PI_{ABS} exhibited an evidently concentration-dependent decrease. Furthermore, there is a highly linear correlation between PI_{ABS} and φ_{Eo} or Q_A-reducing centers in the presence of PAT with different concentrations (Figure 5F). This indicates that PAT-caused inactivation of Q_A-reducing centers due to the blockage of PSII electron transport is the major dominant factor for the loss of the overall photosynthetic activity in PSII.

Considering above results, PAT mainly targets the Q_B site of the D1 protein to block PSII electron transport at the acceptor side.

Modeling of PAT Binding to the D1 Protein. PSII inhibitor herbicides generally target at the PSII acceptor side for the D1 protein and interrupt linear electron transport of

https://doi.org/10.1021/acs.jafc.1c01811
J. Agric. Food Chem. 2021, 69, 7313−7323

photosynthesis by competing with native PQ for the Q_B sites.[40] There are five trans-membrane α-helices and several short nonmembrane helices between these transmembrane helices in the D1 protein of higher plants.[41] The Q_B site, which is also called the PSII herbicide binding site, locates exactly between the helices IV and V of the D1 protein from phenylalanine 211 to leucine 275.[42−44]

To further confirm whether PAT binds to the D1 protein and corroborate the binding properties of PAT within the Q_B site, PAT was modeled to the Q_B site of the *A. adenophora* D1 protein based on the available experimental and theoretical structure information of PSII herbicides binding in the D1 protein by Discovery Studio version 3.5 (Figure 6). The proposed molecular modeling of PAT binding to the D1 protein shows that a major hydrogen bond with a distance of 2.24 Å is formed between the residue D1-His252 and the O2 carbonyl oxygen atom of PAT (Figure 6A and Table 3). The residues D1-His215, D1-Ser264, and D1-Phe265 also form, respectively, an electrostatic interaction with the O4 oxygen atom, C7 carbon atom, and O1 oxygen atom of PAT whose bound distances are 3.11, 2.83, and 3.14 Å (Table 3). In addition, the van der Waals interactions formed between PAT and the residues Phe211, Met214, Leu218, Phe255, Asn266, and Leu271 in the D1 protein also perhaps participate in the complex stabilization of PAT binding to the Q_B site (Figure 6A,B). Surface representation of the Q_B binding site with bound PAT shows that PAT is totally nestled in the cavity formed by the Q_B-binding pocket (Figure 6C). Clearly, PAT is different from classical PSII herbicides in the binding environment despite the fact that they share the common action target as the Q_B site of the D1 protein.

For classical herbicide DCMU, a primary hydrogen bond is formed between the oxygen atom of D1-Ser264 and the N9 amide hydrogen of DCMU. Also, the residue D1-His215 contributes to DCMU binding by providing a weak hydrogen bridge to the carbonyl group of DCMU.[8,42,45] The crystal structure of *Rhodopseudomonas viridis* reaction center complexes with atrazine (5PRC) revealed that atrazine interacts with the Q_B site by a hydrogen bond between the residue D1-Ser264 and its N11 hydrogen and N1 atoms.[43,46] The pattern of hydrogen bonding geometry for the terbutryn-reaction center complexes (1DXR) is very similar to the binding of atrazine and other triazine inhibitors.[47] In the modeling of bromoxynil and ioxynil binding to the Q_B site, a strong hydrogen bond is formed between the phenolate anion and the NH group of D1-His215.[48] Based on the crystallographic investigations and studies on resistant mutants, it is generally accepted that urea/triazine family inhibitors bind to the D1 protein by a key hydrogen bond formed between the Ser264 residue and inhibitor molecules, and the phenolic inhibitors interact with the D1 protein via the His215 residue.[42,46,49,50] In contrast to two classes of PSII herbicides, although the residues D1-His215 and D1-Ser264 are considered to participate in forming a binding pocket for PAT, they cannot provide hydrogen bonding to it (Figure 6C). This may be attributed to the difference of their characteristic chemical group.

Natural photosynthetic inhibiting products reveal more complex binding behaviors in the Q_B site. According to the context of the capsaicin binding site of the *R. viridis* reaction center with capsaicin complexes, the residues His190 and Ser223 in the L-subunit (L) donate hydrogen bonds to capsaicin, which are conserved into D1-His215 and D1-Ser264 in PSII.[14] X-ray crystallographic analysis of structural details of stigmatellin binding to *R. viridis* reaction center complexes suggests that stigmatellin binds to the Q_B site by a hydrogen bond between the proximal methoxy oxygen of stigmatellin and L-His190 and another hydrogen bond between the hydroxyl group of stigmatellin and L-Ser223.[51] Here, the molecular interaction model of PAT binding to the Q_B site indicates that the residue His252 in the D1 protein provides a key ligand to the O2 carbonyl oxygen atom of PAT by forming a hydrogen bond. This is different from the above classical PSII herbicides and natural PSII inhibitors. Therefore, PAT is a novel natural photosynthetic inhibitor and has the potential to be explored as a bioherbicide in the future. However, the accurate binding environment of PAT needs to be further verified by crystallographic data and mutant experiments.

To develop bioherbicides, it is important to explore new natural products with high activity in weed control. Based on the photosynthetic efficiency analysis, it is demonstrated that PAT blocks PSII electron flow further than Q_A at the acceptor side and destroys photosynthetic pigments strongly. By docking PAT to the *A. adenophora* D1 protein, it was found that PAT binds to the Q_B site by forming a hydrogen bond with the residue His252 in the D1 protein, whereas typical herbicides DCMU and atrazine have been shown to form hydrogen bonds with the residue Ser264 in the D1 protein. Therefore, with a novel site of action, PAT has the potential to be developed as a bioherbicide. Based on the structure of PAT, derivatives with more potent herbicidal activities can be designed and assembled to exploit new herbicides in the future.

AUTHOR INFORMATION

Corresponding Author

Shiguo Chen − *Weed Research Laboratory, Nanjing Agricultural University, Nanjing 210095, China;* orcid.org/0000-0002-8762-1373; Phone: +86-25-84395117; Email: chenshg@njau.edu.cn

Authors

Yanjing Guo − *Weed Research Laboratory, Nanjing Agricultural University, Nanjing 210095, China*

Weizhe Liu − *Weed Research Laboratory, Nanjing Agricultural University, Nanjing 210095, China*

He Wang − *Weed Research Laboratory, Nanjing Agricultural University, Nanjing 210095, China*

Xiaoxiong Wang − *Weed Research Laboratory, Nanjing Agricultural University, Nanjing 210095, China; Plant Protection and Quarantine Station, Yangcheng Agricultural and Rural Bureau, Yangcheng 048100, China*

Sheng Qiang − *Weed Research Laboratory, Nanjing Agricultural University, Nanjing 210095, China*

Hazem M. Kalaji − *Department of Plant Physiology, Institute of Biology, Warsaw University of Life Sciences SGGW, Warsaw 02776, Poland*

Reto Jörg Strasser − *Weed Research Laboratory, Nanjing Agricultural University, Nanjing 210095, China; Bioenergetics Laboratory, University of Geneva, Jussy/Geneva 1211, Switzerland*

Complete contact information is available at: https://pubs.acs.org/10.1021/acs.jafc.1c01811

Author Contributions

S.C. designed this research. W.L., Y.G., and X.W. carried out experiments. S.C., W.L., Y.G., H.W., and R.J.S. analyzed the data. Y.G., S.C., and W.L. wrote the paper. S.Q., R.J.S., and

https://doi.org/10.1021/acs.jafc.1c01811
J. Agric. Food Chem. 2021, 69, 7313−7323

H.M.K. revised the manuscript and prepared the final version. Each author has read the paper.

Funding

This research was supported by the National Key Research and Development Program (2017YFD0201300), Open Funs of the State Key Laboratory of Plant Physiology and Biochemistry (SKLPPBKF2118), and Foreign Expert Project (G20190010118).

Notes

The authors declare no competing financial interest.

REFERENCES

(1) Heap, I. Global perspective of herbicide-resistant weeds. *Pest Manage. Sci.* **2014**, *70*, 1306−1315.

(2) Morin, L. Progress in biological control of weeds with plant pathogens. *Annu. Rev. Phytopathol.* **2020**, *58*, 201−223.

(3) Cantrell, C. L.; Dayan, F. E.; Duke, S. O. Natural products as sources for new pesticides. *J. Nat. Prod.* **2012**, *75*, 1231−1242.

(4) Duke, S. O.; Romagni, J. G.; Dayan, F. E. Natural products as sources for new mechanisms of herbicidal action. *Crop Prot.* **2000**, *19*, 583−589.

(5) Frank, E. D.; Stephen, O. D. Natural compounds as next-generation herbicides. *Plant Physiol.* **2014**, *166*, 1090−1105.

(6) Fedtke, C.; Duke, S. O. Herbicides. In *Plant Toxicology* (Fourth Edition); Hock, B.; Elstner, E. F., Eds.; Marcel Dekker: New York, 2005; 247−330.

(7) Oettmeier, W.; Masson, K.; Johanningmeier, U. Evidence for two different herbicide-binding proteins at the reducing side of photosystem II. *Biochim. Biophys. Acta* **1982**, *679*, 376−383.

(8) Trebst, A. The three-dimensional structure of the herbicide binding niche on the reaction center polypeptides of photosystem II. *Z. Naturforsch.* **1987**, *42*, 742−750.

(9) Chen, S.; Xu, X.; Dai, X.; Yang, C.; Qiang, S. Identification of tenuazonic acid as a novel type of natural photosystem II inhibitor binding in Q_B-site of *Chlamydomonas reinhardtii*. *Biochim. Biophys. Acta* **1767**, *2007*, 306−318.

(10) Guo, Y.; Cheng, J.; Lu, Y.; Wang, H.; Gao, Y.; Shi, J.; Yin, C.; Wang, X.; Chen, S.; Strasser, R. J.; Qiang, S. Novel action targets of natural product gliotoxin in photosynthetic apparatus. *Front. Plant Sci.* **2020**, *10*, 1688.

(11) Oettmeier, W.; Godde, D.; Kunze, B.; Höfle, G. Stigmatellin. A dual type inhibitor of photosynthetic electron transport. *Biochim. Biophys. Acta* **1985**, *807*, 216−219.

(12) Mazur, B. J.; Falco, S. C. The Development of herbicide resistant crops. *Annu. Rev. Plant Physiol.* **1989**, *40*, 441.

(13) Nimbal, C. I.; Yerkes, C. N.; Weston, L. A.; Weller, S. C. Herbicidal activity and site of action of the natural product sorgoleone. *Pestic. Biochem. Physiol.* **1996**, *54*, 73−83.

(14) Spyridaki, A.; Fritzsch, G.; Kouimtzoglou, E.; Baciou, L.; Ghanotakis, D. The natural product capsaicin inhibits photosynthetic electron transport at the reducing side of photosystem II and purple bacterial reaction center: structural details of capsaicin binding. *Biochim. Biophys. Acta* **2000**, *1459*, 69−76.

(15) Srivastava, A.; Jüttner, F.; Strasser, R. J. Action of the allelochemical, fischerellin A, on photosystem II. *Biochim. Biophys. Acta* **1998**, *1364*, 326−336.

(16) Ritieni, A. Patulin in Italian commercial apple products. *J. Agric. Food Chem.* **2003**, *51*, 6086−6090.

(17) Zheng, X.; Yang, Q.; Zhang, H.; Cao, J.; Zhang, X.; Apaliya, M. T. The possible mechanisms involved in degradation of patulin by *Pichia caribbica*. *Toxins* **2016**, *8*, 289.

(18) Diao, E.; Hou, H.; Hu, W.; Dong, H.; Li, X. Removing and detoxifying methods of patulin: A review. *Trends Food Sci. Technol.* **2018**, *81*, 139−145.

(19) Adrian, L.; Kashif, J.; Mohanad, Z.; Florian, L. Patulin-induced suicidal erythrocyte death. *Cell. Physiol. Biochem.* **2013**, *32*, 291−299.

(20) Sexena, N.; Ansari, K. M.; Kumar, R.; Dhawan, A.; Dwivedi, P. D.; Das, M. Patulin causes DNA damage leading to cell cycle arrest and apoptosis through modulation of Bax, p^{53} and $p^{21/WAF1}$ proteins in skin of mice. *Toxicol. Appl. Pharm.* **2009**, *234*, 192−201.

(21) Glaser, N.; Stopper, H. Patulin: mechanism of genotoxicity. *Food Chem. Toxicol.* **2012**, *50*, 1796−1801.

(22) Norstadt, F. A.; Mccalla, T. M. Effects of patulin on wheat grown to maturity. *Soil Sci.* **1971**, *111*, 236−243.

(23) Lô-Pelzer, E.; Aubertot, J. N.; Bousset, L.; Pinochet, X.; Jeuffroy, M. H. Phoma stem canker (*Leptosphaeria maculans/L. biglobosa*) of oilseed rape (*Brassica napus*): is the G_2 disease index a good indicator of the distribution of observed canker severities? *Eur. J. Plant Pathol.* **2009**, *125*, 515−522.

(24) Gao, Y.; Liu, W.; Wang, X.; Yang, L.; Han, S.; Chen, S.; Strasser, R. J.; Valverde, B. E.; Qiang, S. Comparative phytotoxicity of usnic acid, salicylic acid, cinnamic acid and benzoic acid on photosynthetic apparatus of *Chlamydomonas reinhardtii*. *Plant Physiol. Biochem.* **2018**, *128*, 1−12.

(25) Coombs, J.; Hall, D. O.; Long, S. P.; Scurlock, J. M. O. Techniques in Bioproductivity and Photosynthesis. *Beijing, Science Press* **1986**, 142−144.

(26) Chen, S.; Yin, C.; Dai, X.; Qiang, S.; Xu, X. Action of tenuazonic acid, a natural phytotoxin, on photosystem II of spinach. *Environ. Exp. Bot.* **2008**, *62*, 279−289.

(27) Strasser, R. J.; Tsimilli-Michael, M.; Srivastava, A. Analysis of the Chlorophyll a Fluorescence Transient. In *Chlorophyll Fluorescence: A Signature of Photosynthesis*; Papageorgiou, G. C.; Govindjee, Eds.; Kluwer Academic Publishers: Netherlands, 2004; 321−362.

(28) Chen, S.; Strasser, R. J.; Qiang, S. *In vivo* assessment of effect of phytotoxin tenuazonic acid on PSII reaction centers. *Plant Physiol. Biochem.* **2014**, *84*, 10−21.

(29) Waterhouse, A.; Bertoni, M.; Bienert, S.; Studer, G.; Tauriello, G.; Gumienny, R.; Heer, F. T.; de Beer, T. A. P.; Rempfer, C.; Bordoli, L.; Lepore, R.; Schwede, T. SWISS-MODEL: homology modelling of protein structures and complexes. *Nucleic Acids Res.* **2018**, *46*, W296−W303.

(30) Chen, S.; Yang, J.; Zhang, M.; Strasser, R. J.; Qiang, S. Classification and characteristics of heat tolerance in *Ageratina adenophora* populations using fast chlorophyll a fluorescence rise O-J-I-P. *Environ. Exp. Bot.* **2016**, *122*, 126−140.

(31) Govindjee; Shevela, D.; Björn, L. O. Evolution of the Z-scheme of photosynthesis: a perspective. *Photosynth. Res.* **2017**, *133*, 5−15.

(32) Strasser, R. J.; Srivastava, A.; Govindjee. Polyphasic chlorophyll *a* fluorescence transient in plants and cyanobacteria. *Photochem. Photobiol.* **1995**, *61*, 32−42.

(33) Strasser, R. J.; Govindjee. The F_O and the O-J-I-P fluorescence rise in higher plants and algae. In *Regulation of Chloroplast Biogenesis*; Argyroudi-Akoyunoglou, J. H., Ed.; Plenum Press: New York, 1992; 423−426.

(34) King-Díaz, B.; Pérez-Reyes, A.; Santos, F. J. L. D.; Ferreira-Alves, D. L.; Veloso, D. P.; Carvajal, S. U.; Lotina-Hennsen, B. Natural diterpene β-lactone derivative as photosystem II inhibitor on spinach chloroplasts. *Pestic. Biochem. Phys.* **2006**, *84*, 109−115.

(35) Srivastava, A.; Strasser, R. J. How do land plants respond to stress temperature and stress light? *Archs. Sci. Genève* **1995**, *48*, 135−146.

(36) Srivastava, A.; Guissé, B.; Greppin, H.; Strasser, R. J. Regulation of antenna structure and electron transport in photosystem II of *Pisum sativum* under elevated temperature probed by the fast polyphasic chlorophyll *a* fluorescence transient: OKJIP. *Biochim. Biophys. Acta* **1997**, *1320*, 95−106.

(37) Krause, G. H.; Weis, E. Chlorophyll fluorescence and photosynthesis: the basics. *Annu. Rev. Plant Physiol. Plant Mol. Biol.* **1991**, *42*, 313−349.

(38) Tóth, S. Z.; Schansker, G.; Strasser, R. J. In intact leaves, the maximum fluorescence level (F_M) is independent of the redox state of the plastoquinone pool: A DCMU-inhibition study. *Biochim. Biophys. Acta* **2005**, *1708*, 275−282.

https://doi.org/10.1021/acs.jafc.1c01811
J. Agric. Food Chem. 2021, 69, 7313−7323

(39) Lazár, D.; Brokeš, M.; Nauš, J.; Dvořák, L. Mathematical modeling of 3-(3′,4′-dichlorophenyl)-1,1-dimethylurea action in plant leaves. *J. Theor. Biol.* **1998**, *191*, 79−86.
(40) Oettmeier, W. Herbicide resistance and supersensitivity in photosystem II. *Cell. Mol. Life Sci.* **1999**, *55*, 1255−1277.
(41) Kamiya, N.; Shen, J. R. Crystal structure of oxygen-evolving photosystem II from *Thermosynechococcus vulcanus* at 3.7-Å resolution. *Proc. Natl. Acad. Sci. U. S. A.* **2003**, *100*, 98−103.
(42) Xiong, J.; Jee, G.; Subramaniam, S. Modeling of the D1/D2 proteins and cofactors of the photosystem II reaction center: Implications for herbicide and bicarbonate binding. *Protein Sci.* **1996**, *5*, 2054−2073.
(43) Trebst, A. The Mode of Action of Triazine Herbicides in Plants. In *The Triazine Herbicides*; LeBaron, H. M.; McFarland, J. E.; Burnside, O. C., Eds.; Elsevier: San Diego, California, 2008, *8*, 101−110.
(44) Umena, Y.; Kawakami, K.; Shen, J.-R.; Kamiya, N. Crystal structure of oxygen-evolving photosystem II at a resolution of 1.9 Å. *Nature* **2011**, *473*, 55−60.
(45) Sinning, I. Herbicide binding in the bacterial photosynthetic reaction center. *Trends Biochem. Sci.* **1992**, *17*, 150−154.
(46) Lancaster, C. R. D.; Michel, H. Refined crystal structures of reaction centres from *Rhodopseudomonas viridis* in complexes with the herbicide atrazine and two chiral atrazine derivatives also lead to a new model of the bound carotenoid. *J. Mol. Biol.* **1999**, *286*, 883−898.
(47) Lancaster, C. R. D.; Bibikova, M. V.; Sabatino, P.; Oesterhelt, D.; Michel, H. Structural basis of the drastically increased initial electron transfer rate in the reaction center from a *Rhodopseudomonas viridis* mutant described at 2.00-Å resolution. *J. Biol. Chem.* **2000**, *275*, 39364−39368.
(48) Takahashi, R.; Hasegawa, K.; Takano, A.; Noguchi, T. Structures and binding sites of phenolic herbicides in the Q_B pocket of photosystem II. *Biochemistry* **2010**, *49*, 5445−5454.
(49) Mackay, S. P.; O'Malley, P. J. Molecular modeling of the interactions between DCMU and the Q_B-binding site of photosystem II. *Z. Naturforsch.* **1993**, *48c*, 191−198.
(50) Mackay, S. P.; O'Malley, P. J. Molecular modeling of the interactions between optically active triazine herbicides and photosystem II. *Z. Naturforsch.* **1993**, *48c*, 474−481.
(51) Lancaster, C. R. D.; Michel, H. The coupling of light-induced electron transfer and proton uptake as derived from crystal structures of reaction centres from *Rhodopseudomonas viridis* modified at the binding site of the secondary quinone Q_B. *Structure* **1997**, *5*, 1339−1359.

https://doi.org/10.1021/acs.jafc.1c01811
J. Agric. Food Chem. 2021, 69, 7313−7323